Aerosol Radiative Forcing Derived from SeaWiFS-Retrieved Aerosol Optical Properties

MING-DAH CHOU

NASA Goddard Space Flight Center, Greenbelt, Maryland

PUI-KING CHAN

Science Systems and Applications, Inc., Lanham, Maryland

MENGHUA WANG

University of Maryland Baltimore County, Baltimore, Maryland, and NASA Goddard Space Flight Center, Greenbelt, Maryland

(Manuscript received 29 December 2000, in final form 8 March 2001)

ABSTRACT

To understand climatic implications of aerosols over global oceans, the aerosol optical properties retrieved from the Sea-viewing Wide Field-of-view Sensor (SeaWiFS) are analyzed, and the effects of the aerosols on the earth's radiation budgets [aerosol radiative forcing (ARF)] are computed using a radiative transfer model. It is found that the distribution of the SeaWiFS-retrieved aerosol optical thickness is distinctively zonal. The maximum in the equatorial region coincides with the intertropical convergence zone, and the maximum in the Southern Hemispheric high latitudes coincides with the region of prevailing westerlies. The minimum aerosol optical thickness is found in the subtropical high pressure regions, especially in the Southern Hemisphere. These zonal patterns clearly demonstrate the influence of atmospheric circulation on the oceanic aerosol distribution.

Over global oceans, aerosols reduce the annual-mean net downward solar flux by 5.4 W m^{-2} at the top of the atmosphere, and by 5.9 W m^{-2} at the surface. The largest ARF is found in the tropical Atlantic, Arabian Sea, Bay of Bengal, the coastal regions of Southeast and East Asia, and the Southern Hemispheric high latitudes. During the period of the big Indonesian fires (September–December 1997), the cooling due to aerosols is more than 10 W m^{-2} at the top of the atmosphere, and more than 25 W m^{-2} at the surface in the vicinity of Indonesia. The atmosphere receives extra solar radiation by more than 15 W m^{-2} over a large area. These large changes in radiative fluxes are expected to have enhanced the atmospheric stability, weakened the atmospheric circulation, and augmented the drought condition during that period. It would be very instructive to simulate the regional climatic impact of the big Indonesian fires during the 1987–88 El Niño event using a general circulation model.

1. Introduction

Aerosols directly affect the heat budgets of the earth by reflecting and absorbing solar radiation. The lifetime of aerosols is short, and the temporal and spatial variations are large. As a result, information on long-term and global distributions of aerosols is lacking, and the climatic impact of aerosols is not well understood.

Satellite remote sensing of aerosols over land is difficult because the reflectivity of aerosols is usually smaller than the reflectivity of land surface. Over oceans, the surface reflectivity is small and aerosol optical properties can be estimated much more reliably than that over land. The Total Ozone Mapping Spectrometer (TOMS) retrieves the aerosol distribution over both land and oceans by means of aerosol index, which is related to the aerosol optical thickness and the single scattering albedo (Herman et al. 1997). Distributions of aerosols over global oceans have been derived from various satellite radiance measurements. For example, Husar et al. (1997) retrieved the aerosol optical thickness from the radiance measured in the 0.63-μm channel of the National Oceanic and Atmospheric Administration Advanced Very High Resolution Radiometer (AVHRR). Michchenko et al. (1999) applied a two-channel retrieval algorithm to the AVHRR measurements and derived both the optical thickness and the Ångström exponent, which provides information on the spectral variation of the optical thickness. Deuze et al. (1999) retrieved the aerosol optical thickness and the Ångström exponent from the radiances and polarization measured in the 0.670-μm and the 0.865-μm channels of the Polarization and Directionality of the Earth's Reflectances (POLDER) instrument on the Japanese Advanced Earth Observing System. Recently, Rajeev et al. (2000) retrieved the aerosol optical thickness over the Arabian

Corresponding author address: Dr. Ming-Dah Chou, NASA Goddard Space Flight Center, Code 913, Greenbelt, MD 20771.
E-mail: chou@climate.gsfc.nasa.gov

Sea, the Bay of Bengal, and the Indian Ocean using the radiance measured in the 0.63-μm channel of the AVHRR. The retrieval used an aerosol model constructed from the aerosol chemical, microphysics and optical properties measured at the Kaashidhoo Climate Observatory on the island of Kaashidhoo (4.96°N, 73.46°E) during the Indian Ocean Experiment. In addition to satellite retrievals, the global distribution of aerosols has also been simulated using models. Chin et al. (2002), Haywood et al. (1999), and Tegen et al. (2000) derived the global distributions of optical properties of various aerosol types using a chemistry–aerosol–transport model driven by model simulated/assimilated atmospheric temperature, humidity, and cloud fields. The products include not only the optical thickness but also the single scattering albedo and asymmetry factor, all of which are important for computing the radiative effect of aerosols [or aerosol radiative forcing (ARF)].

The National Aeronautics and Space Administration (NASA) launched the Sea-viewing Wide Field-of-view Sensor (SeaWiFS) satellite on 1 August 1997 to measure global ocean color and to retrieve ocean bio-optical properties (Hooker et al. 1992). The retrieved aerosol optical thickness over global oceans is a by-product of the SeaWiFS atmospheric correction for ocean color products (Gordon and Wang 1994b). The aerosol data are available starting from September 1997. The SeaWiFS is a polar orbiting satellite with an equatorial crossing at local noon, and the temporal resolution of the retrieved aerosol optical thickness and Ångström exponent is once a day (Wang et al. 2000a). It has a high spatial resolution of 1 km at the nadir.

In this study, we conduct radiative transfer calculations to assess the radiative forcing of aerosols retrieved from the SeaWiFS radiance measurements. The SeaWiFS algorithm for retrieving oceanic aerosols is summarized in section 2. The radiative transfer model used for calculating ARF and the source of data used for input to the radiation model are described in section 3. Section 4 analyzes the distribution of the SeaWiFS-retrieved aerosol over global oceans and its relation to atmospheric circulation. Section 5 presents the results of model-calculated ARF at the top of the atmosphere (TOA), in the atmosphere, and at the surface. Comparisons of the model-calculated clear-sky solar flux at TOA with satellite retrievals are given in section 6. Conclusions of this work are given in section 7.

2. The SeaWiFS aerosol retrieval algorithm

The total upward radiance at the top of the ocean–atmosphere system $L_t(\lambda)$ measured at the two SeaWiFS near-infrared (NIR) wavelengths at 0.765 μm and 0.865 μm can be written as

$$L_t(\lambda) = L_r(\lambda) + L_a(\lambda) + L_{ra}(\lambda) + tL_{wc}(\lambda) + TL_g(\lambda), \quad (1)$$

where $L_r(\lambda)$, $L_a(\lambda)$, and $L_{ra}(\lambda)$ are the radiance contributions from multiple scattering of air molecules (Rayleigh scattering with no aerosols), aerosols (no molecules), and Rayleigh–aerosol interactions, respectively (Gordon and Wang 1994b). The specular reflection from the direct sun (sun glint) radiance is $L_g(\lambda)$, and $L_{wc}(\lambda)$ is the radiance at the sea surface resulting from sunlight and skylight reflecting off whitecaps on the surface (Gordon and Wang 1994a); T and t are the atmospheric direct and diffuse transmittances (Yang and Gordon 1997) at the sensor viewing direction, respectively. For clear ocean waters, the radiance contributions from ocean water are negligible at the two NIR bands because of strong water absorption. For productive ocean waters, radiances from waters at the two NIR bands are estimated using a bio-optical model (Siegel et al. 2000). In the above equation, the Rayleigh radiances $L_r(\lambda)$ are computed using the vector radiative transfer theory (accounting for polarization) for a Rayleigh-scattering atmosphere overlying a rough (wind speed-dependent) Fresnel-reflecting ocean surface (Gordon and Wang 1992). The whitecap radiances are computed using a model with input of sea surface wind speed (Gordon and Wang 1994a), and the sun glint contamination is minimized by operationally tilting the sensor 20° away from the nadir at subsolar point, applying a sun glint mask, and making an explicit correction for residual contamination. The aerosol radiances $L_a(\lambda) + L_{ra}(\lambda)$ are generated as lookup tables (12 aerosol models; Gordon and Wang 1994b) based on aerosols from Shettle and Fenn (1979). The SeaWiFS aerosol retrieval algorithm uses the aerosol radiances measured at the 0.765- and 0.865-μm channels, that is, $L_t(\lambda) - L_r(\lambda) - tL_{wc}(\lambda) - TL_g(\lambda)$, to select the two most appropriate aerosol models from a suite of 12 candidate aerosol models. The aerosol optical thickness is then retrieved from the radiance at 0.865 μm.

Wang et al. (2000b) compared the SeaWiFS-derived aerosol optical thickness at 0.865 μm with that derived from ground radiance measurements using both Cimel sun–sky scanning radiometer within the Aerosol Robotic Network (AERONET—Holben et al. 1998) and handheld MICROTOPS sun photometers. Figure 1 shows that the SeaWiFS-derived aerosol optical thicknesses are in good agreement with the CIMEL measurements at various coastal and island stations.

3. Radiative transfer model and data source

The effects of aerosols on the solar radiation (or ARF) at TOA, in the atmosphere, and at the surface are calculated using the radiation model of Chou and Suarez (1999). Calculations of clear-sky solar fluxes include the absorption of solar radiation by ozone, water vapor, CO_2, and O_2, scattering due to gases (Rayleigh scattering), and the absorption and scattering due to aerosols. Interactions among gas absorption, Rayleigh scattering, aerosol scattering and absorption, and surface

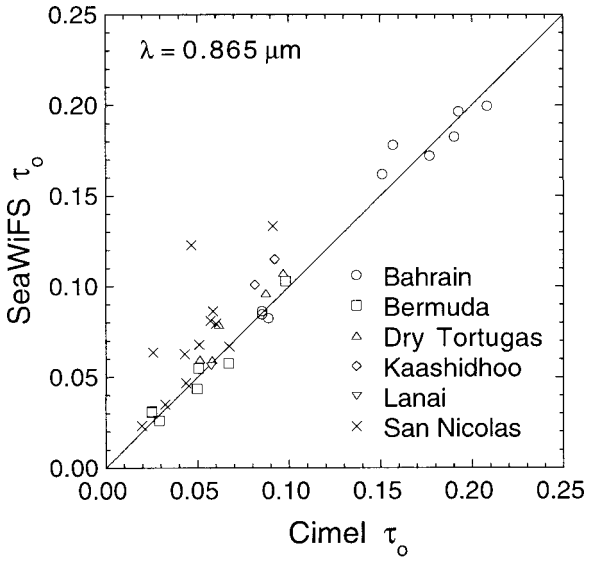

FIG. 1. The SeaWiFS-retrieved aerosol optical thickness at 0.865 μm compared with that retrieved from radiance measurements at various AERONET stations (from Fig. 26d of Wang et al. 2000b).

reflection are explicitly included using the δ-Eddington approximation. The solar spectrum is divided into the ultraviolet (UV)–visible region (0.175–0.7 μm) and the infrared (IR) region (0.7–10 μm). The UV and visible region is further divided into 8 bands, and the IR region is divided into 3 bands. Single values of the ozone absorption coefficient, Rayleigh scattering coefficient, and aerosol optical properties (optical thickness, single scattering albedo, asymmetry factor) are used for each band. The absorption in the IR due to water vapor is computed using the *k*-distribution method, where *k* is the absorption coefficient. Ten values of *k* are used in each of the three IR bands, whereas a single value of *k* is applied to computing the water vapor absorption in the photosynthetically active region from 0.4 to 0.7 μm.

Data input to the radiation model for clear-sky flux calculations include vertical profiles of temperature, humidity, ozone, the aerosol optical properties, and the albedo of the ocean surface. The temperature fields are taken from the National Centers for Environmental Prediction–National Center for Atmospheric Research (NCEP–NCAR) reanalysis (Kalnay et al. 1996). The column water vapor is taken from the Special Sensor Microwave Imager (SSM/I) retrievals of Wentz (1994). The column ozone amounts are taken from the TOMS retrievals (McPeters et al. 1998), which are climatological monthly mean values. To justify the use of climatological monthly ozone amount, we have conducted model sensitivity studies. Model calculations show that fluxes at the TOA and the surface are not sensitive to the ozone amount. The daily mean surface flux in the Tropics changes by less than 0.5 W m^{-2} when the column ozone amount changes from 250 Dobson units to 320 Dobson units. The former is a typical ozone amount of equatorial regions, and the latter is typical of subtropical regions. The shapes of vertical profiles of water vapor and ozone also have little effect on the absorption of solar radiation. These profiles are assumed to follow that of a typical midlatitude summer atmosphere by scaling the column water vapor and ozone amounts, so that the column amounts are the same as that of the SSM/I- and TOMS-retrieved values. The albedo of the ocean surface is fixed at 0.05, which is assumed to be the mean albedo averaged over solar zenith angles and over both direct and diffuse downward solar fluxes at the surface.

The spectral variation of the aerosol optical thickness is a function of the particle size. For the SeaWiFS maritime aerosol model, the optical thickness relative to that at 0.865 μm is approximated by

$$\frac{\tau_\lambda}{\tau_o} = \left(\frac{\lambda}{\lambda_o}\right)^{-a}, \tag{2}$$

where τ is the optical thickness, λ is the wavelength, $\lambda_o = 0.865$ μm, and τ_o is the optical thickness at λ_o. The parameter a is the Ångström exponent, which is approximately equal to 0.215 for the SeaWIFS maritime aerosols. Usually the parameter a near the highly polluted continents is larger than that over open oceans due to a smaller particle size. We have investigated the sensitivity of the ARF to the particle size by increasing the value of a from 0.215 to 0.5. When the SeaWiFS-retrieved aerosols are used, the effect of a on both the TOA and the surface ARF is negligible. The maximum effect is only 0.5 W m^{-2} and is restricted to very small oceanic regions. The reason for this small effect is the cancellation between the contributions from spectral regions with wavelengths greater and less than 0.865 μm. When a changes from 0.215 to 0.5, the aerosol optical thickness increases in the spectral region $\lambda < 0.865$ μm and decreases in the region $\lambda > 0.865$ μm. The results on ARF shown in this study are calculated using $a = 0.215$.

The asymmetry factor g varies slightly with aerosol models and spectral bands. For the maritime aerosols, the variation of g with wavelength is in the range 0.783–0.790. Therefore, we fix the value of g at 0.786 in calculating ARF. The single scattering albedo affects significantly the ARF, especially at the surface. Over the vast oceanic regions, most of the aerosols are maritime in nature, and sulfuric aerosols can be assumed as typical over oceanic regions. For maritime sulfuric aerosols, the absorption is weak, and we fix the single scattering albedo ω_o at 0.9955 in the model calculations, which is practically nonabsorbing. For aerosols in regions of active tropical forest fires and in the windward side of major deserts, the optical thickness is large. The absorption of solar radiation by these aerosols is strong. The magnitude of ω_o is in the range of 0.88–0.9 (Gras et al. 1999; Podgorny et al. 2000; Tegen et al. 1996). Due to lack of detailed information on the absorption

property of oceanic aerosols, we assume that $\omega_o = 0.9955$ and $g = 0.786$ for $\tau_o < 0.18$ to represent maritime aerosols and $\omega_o = 0.9$ and $g = 0.69$ for $\tau_o > 0.3$ to represent dusts from deserts and smoke from forest fires. For $0.18 < \tau_a < 0.3$, ω_o and g are interpolated linearly with τ_o. The dependence of ω_o and g on spectral band is neglected, again due to the lack of detailed information.

Aerosols are assumed to be evenly distributed between the surface and the 800-hPa level. Model calculations show that the ARF is not sensitive to the vertical extent of aerosols. When the upper boundary of the aerosol layer is changed from 800 to 900 hPa, the ARF at TOA changes by less than 5%.

Using the high temporal resolution (15 min) aerosol optical thickness inferred from radiances at AERONET sites over the globe, Kaufman et al. (2000) found that aerosol optical thickness measured by NASA's *Terra* and Aqua polar-orbiting satellites could represent the daily mean optical thickness with an error of less than 2%. The local time of satellite passing is 1000–1130 for the former and 1230–1400 for the latter. Based on this finding, we have assumed that the SeaWiFS-derived aerosol optical thickness during the local hours 1130–1230 is representative of daily mean values. The solar fluxes are computed at 30-min intervals. The solar zenith angle is computed as a function of local time, day, and latitude. The ARFs presented in the study are mean values averaged over both day and night.

To understand the aerosol distribution over global oceans, we also have computed the global distribution of the divergence of wind. The wind field of the NCEP–NCAR reanalysis is used in this study. Finally, the clear-sky TOA flux derived from the Clouds and the Earth's Radiant Energy System (CERES; Wielicki et al. 1996) is used for the comparison with the model-calculated clear-sky solar flux at TOA.

4. Distribution of aerosol optical thickness over global oceans

The SeaWiFS-retrieved aerosol optical thickness at 0.865 μm τ_o is shown in Fig. 2 for October 1997, January 1998, April 1998, and July 1998. To relate the aerosol distribution to the atmospheric circulation, the divergence of winds at 925 hPa derived from the NCEP–NCAR reanalysis is also shown in the figure for the same months. The most striking feature is that the aerosol distribution is largely zonal. High optical thickness is found in tropical oceans and at high latitudes in the Southern Hemisphere. Low optical thickness is found in the subtropics of both hemispheres. This distribution pattern basically coincides with atmospheric circulation: high in convergence regions and low in divergence regions. The large aerosol optical thickness in the tropical Atlantic is found in all seasons. It is a well-acknowledged feature, as can be seen from satellite images (http://toms.gsfc.nasa.gov/aerosols), that is related primarily to the Sahara Desert dusts and secondarily to African forest fires. The prevailing easterly winds bring the aerosols across the Atlantic to the east coasts of Central and South America.

The maximum in equatorial oceans was not previously well-acknowledged. The maximum in the western Pacific just north of the equator (~10°N) is also shown in the TOMS retrieval, but not the POLDER retrieval (Chiapello et al. 2000). The AVHRR retrieval also found a maximum in this region in March, April, and May 1989–91, but was not as evident in other months (Husar et al. 1997). The question arises concerning the source of the aerosols, especially over the central equatorial Pacific. It is possible that the maximum over equatorial oceans is caused by the convergence of aerosols from subtropical regions in a way similar to the convergence of water vapor. Strong trade winds in the Tropics could produce a substantial amount of sea salt and carry the aerosols to the equatorial region. The types of aerosols in the equatorial region could provide critical information on the source of aerosols. Unfortunately, little information is available.

In January 1998, a narrow band of minimum τ_o is found near the equator over the Pacific, Atlantic, and Indian Oceans. It is consistent with the intertropical convergence zone (ITCZ), which is also shown in the panel on the right-hand side of the same figure. According to the NCEP–NCAR reanalysis, this ITCZ is also the zone of maximum precipitation (not shown in the figure). It is likely that the minimum is related to the removal of aerosols by rain. Other months do not show this feature. It is interesting to note that normally one would concern that the aerosol optical thickness might be overestimated in the ITCZ because of the difficulty in detecting thin or remnants of clouds in a satellite field of view. Apparently, this is not a problem for the SeaWiFS aerosol retrieval for the month of January 1998.

The large value of τ_o in the Arabian Sea and the Bay of Bengal is found in April and July 1998, which is believed to be contributed from fossil fuel combustion and wind-blown dusts. The July maximum of τ_o in the Arabian Sea is also evident in the retrievals using the AVHRR radiance measurements (Husar et al. 1997; Mishchenko et al. 1999). In aerosol retrievals using the AVHRR measurements, Rajeev et al. (2000) found that, in January 1998, the optical thickness in the Arabian Sea and the Bay of Bengal is high (0.15–0.45 at 630 μm). This feature is not found in the SeaWiFS retrieval. Part of the reason for this discrepancy might be due to the limit imposed in the SeaWiFS-retrieval algorithm that no retrievals are made for $\tau_o > 0.5$.

In the northern spring, a large amount of desert dust and aerosol from fossil fuel combustion is carried by prevailing westerly winds from Asia across the North Pacific to the west coast of North America. Measurements from TOMS shows that it takes ~5–6 days for aerosols to transport across the North Pacific at ~45°–55°N (http://toms.gsfc.nasa.gov/aerosols). The local

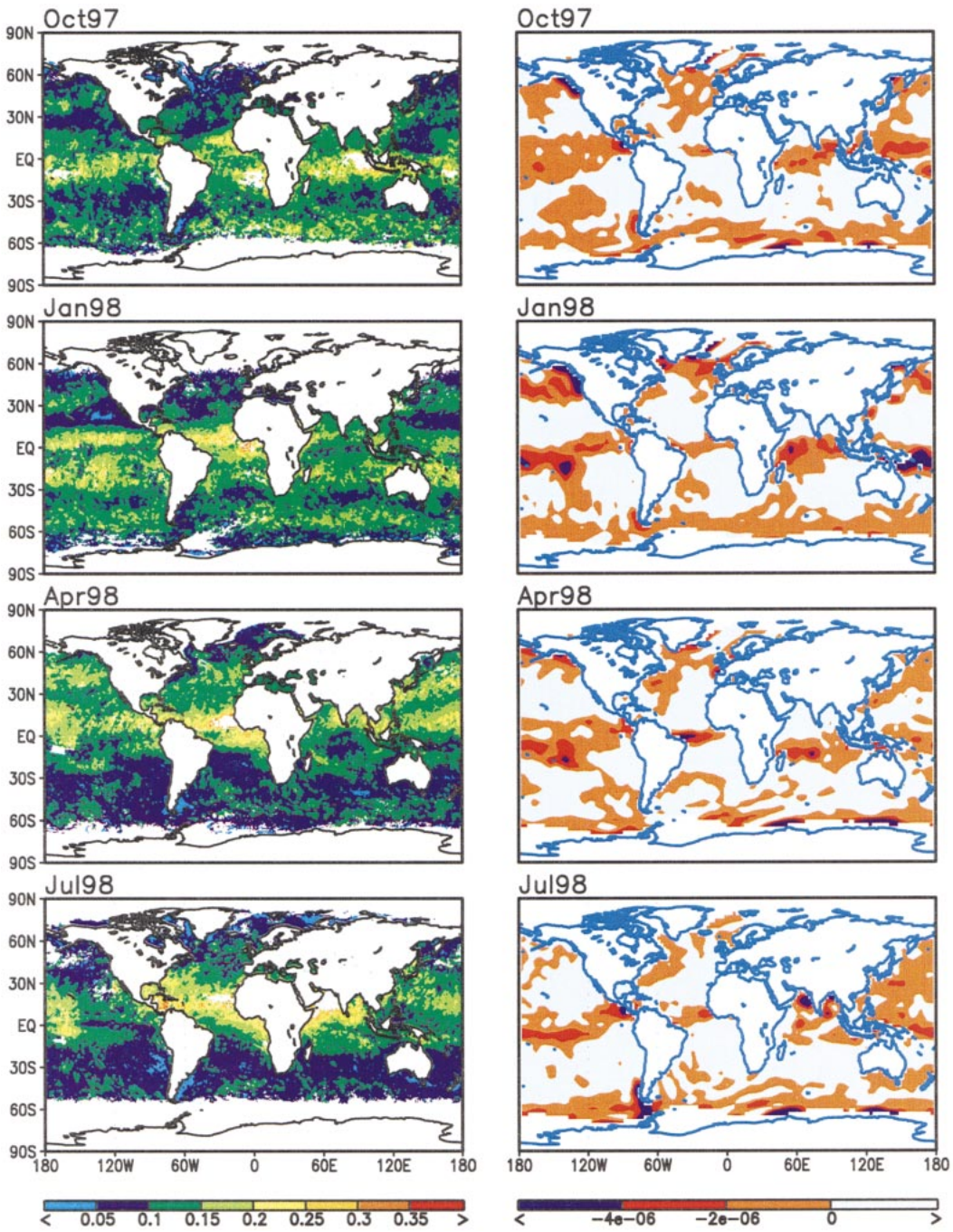

FIG. 2. The SeaWiFS-retrieved aerosol optical thickness at 0.865 μm (left panels) and the divergence of winds at 925 hPa derived from the NCEP–NCAR reanalysis (right panels). (Units of the wind divergence: s^{-1}.)

maximum aerosol optical thickness in the North Pacific during April 1998, as shown in Fig. 2, is likely related to the aerosols from Asia.

During the period September–November 1997, there were big forest fires in Indonesia. The period of the big Indonesian fires coincides with the 1997–98 El Niño when the convection center in the Maritime Continent shifted eastward to the central equatorial Pacific, and Indonesia was under the influence of subsiding air, which augmented the forest fires. The large value of τ_o is shown clearly in the SeaWiFS retrievals (top-left panel), which extends from the Maritime Continent westward to the equatorial Indian Ocean.

In the SH, the maximum at high latitudes, centered at 50°–60°S, is related to a large amount of sea salt and maritime sulfuric aerosols generated by strong prevail-

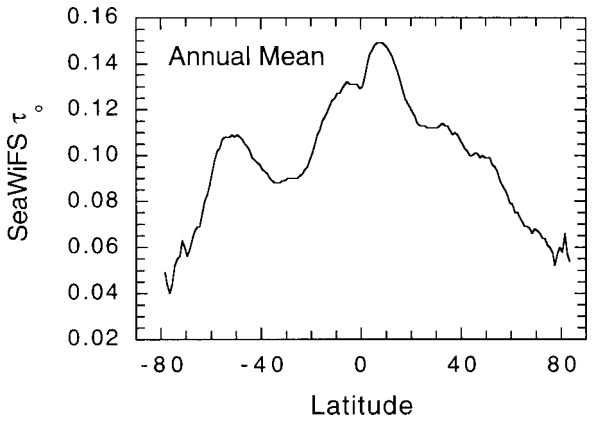

FIG. 3. Latitudinal distribution of the SeaWiFS-retrieved aerosol optical thickness at 0.865 μm over oceans for the year 1998.

ing westerlies. This maximum aerosol band is also shown in the study of Chin et al. (2002) using a chemical model coupled to the atmospheric circulation simulated by the Data Assimilation Office of NASA Goddard Space Flight Center. The minimum in the subtropical zone, centered at 30°S, is also evident in Husar et al. (1997) and Mishchenko et al. (1999).

Figure 3 shows the latitudinal distribution of SeaWiFS-retrieved aerosol optical thickness over oceans for the year 1998. The maxima in the ITCZ and at southern high latitudes (50°–60°S), as well as the minimum in the southern subtropical high pressure region (20°–30°S) are evident. The minimum at the northern subtropical high pressure region (~25°N) is not as evident. Averaged over global oceans, both mean and median τ_o are 0.105. The region with $\tau_o > 0.25$ is very small (not shown in the figures).

5. Aerosol radiative forcing

The effects of aerosols on the radiative fluxes, defined as the radiative forcing, at TOA and the surface are given by

$$\Delta F_t^{\downarrow} = F_{t,dst}^{\downarrow} - F_{t,cln}^{\downarrow}, \quad \text{and} \tag{3}$$

$$\Delta F_s^{\downarrow} = F_{s,dst}^{\downarrow} - F_{s,cln}^{\downarrow}, \tag{4}$$

where $F^{\downarrow}$ denotes the net downward flux (downward minus upward radiation integrated over the solar spectrum); the subscripts ''t'' and ''s'' denote TOA and the surface; and ''dst'' and ''cln'' denote dusty and clean skies, respectively.

The ARFs at TOA and the surface, averaged over the year 1998, are shown in Fig. 4. The ARFs are first calculated for each day and each 1° × 1° latitude–longitude region, then averaged over the year. Large aerosol cooling of the ocean–atmosphere system (upper panel) exceeding 6 W m^{-2} is found in the tropical Atlantic, central equatorial Pacific, Southern Hemispheric high latitudes, and the coastal regions extending from East

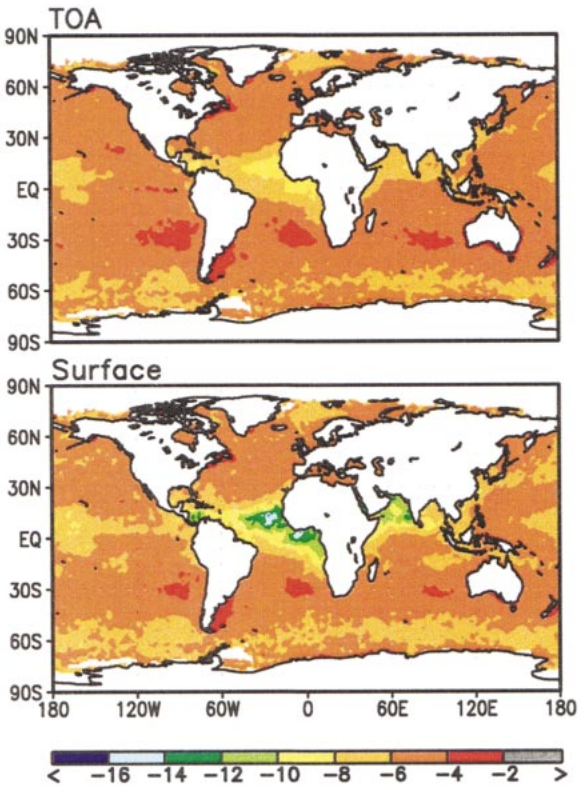

FIG. 4. The model-calculated aerosol radiative forcing at the TOA (upper panel) and at the surface (lower panel) averaged over the year 1998. (Units: W m^{-2}.)

Africa, Arabian Sea, Bay of Bengal, Southeast Asia, to East Asia. In the eastern tropical Atlantic, the maximum cooling exceeds 8 W m^{-2} due to aerosols from Sahara dust and forest fires. The minimum cooling is located in the subtropics, especially in the SH where the cooling is less than 4 W m^{-2}.

The lower panel of Fig. 4 shows the annual-mean ARF at the surface. The distribution of ARF at the surface follows closely the ARF at the TOA. In the tropical Atlantic and the Arabian Sea, the forcing at the surface is much larger than that at TOA, with a maximum cooling of ~15 W m^{-2}. By taking the difference between the forcing at TOA and the surface, it follows that aerosols in these regions enhance the solar heating of the atmosphere by ~4 W m^{-2}. It is noted that the large surface ARF in the tropical Atlantic and the Arabian Sea occurs primarily in the summer months of May–September 1998.

The largest ARF occurs in the eastern portion of the tropical Atlantic and spreads westward to the east coasts of Central America and northern South America. High ARF is found throughout the whole year. The large aerosol forcing is expected to have a significant effect on cloud dynamics, the atmospheric stability, and the atmospheric circulation in the tropical Atlantic. In the Arabian Sea and the Indian Ocean, large aerosol forcing

TABLE 1. Aerosol radiative forcing over oceans for 1998. (Units: W m^{-2}.)

	Jan	Apr	Jul	Oct	Annual
			TOA		
NH	−5.2	−6.7	−6.1	−4.8	−5.7
SH	−6.6	−4.2	−3.9	−5.8	−5.1
Global	−6.0	−5.2	−4.9	−5.3	−5.4
			Surface		
NH	−5.7	−7.8	−7.4	−5.1	−6.5
SH	−7.2	−4.4	−4.1	−6.2	−5.5
Global	−6.6	−5.8	−5.6	−5.7	−5.9

is found in the spring and summer (from April through September).

Table 1 shows the aerosol radiative forcing averaged over oceans in January, April, July, October, and the whole year of 1998. The seasonal change in ARF is large. The maximum and minimum of the monthly mean ARF differ by ~33% in the Northern Hemisphere (NH) and ~50% in the SH. The seasonal variation of the incoming solar radiation at TOA is larger at high latitudes than at low latitudes. Because there is larger fractional oceanic coverage at high latitudes in the SH than in the NH, the seasonal variation of ARF in the SH is larger than the NH. Averaged over global oceans, the annual mean ARF is −5.4 W m^{-2} at TOA and −5.9 W m^{-2} at the surface. Aerosols enhance the atmospheric solar heating by 0.5 W m^{-2}.

Nearly all of previous studies on large-scale ARF were based on model simulations of aerosol distributions. Among those studies, only a few included all major aerosol species. Still, some included both land and ocean and both clear and cloudy skies (e.g. Tegen et al. 2000). As a result, direct comparisons of our results with most of other studies are difficult. Haywood et al. (1999) derived the distributions of major aerosol species over global oceans using a chemistry/transport model and computed the clear-sky ARF. For the period 1987–88, they estimated the clear-sky ARF over global oceans to range from −8.7 to −5.1 W m^{-2} at TOA and from −10.8 to −7.4 W m^{-2} at the surface. The magnitudes of these ARFs are larger than our calculations. Boucher and Tanre (2000) computed the TOA ARF over global oceans using the aerosol optical thickness retrieved from the POLDER radiance measurements. They found that the mean TOA ARF over global oceans is nearly constant (~−5.7 W m^{-2}) during the 8 months between November 1996 and June 1997. The mean ARF is very close to our result of −5.4 W m^{-2}. However, the TOA ARF in the NH is larger than the SH by 2–4 W m^{-2} which is due to the much larger POLDER-retrieved aerosol optical thickness in the NH than in the SH (Deuze et al. 1999). We do not find such a large difference between the two hemispheres when the SeaWiFS aerosols are used (Table 1).

As can be expected, the latitudinal distribution of ARF changes significantly with seasons due to changes

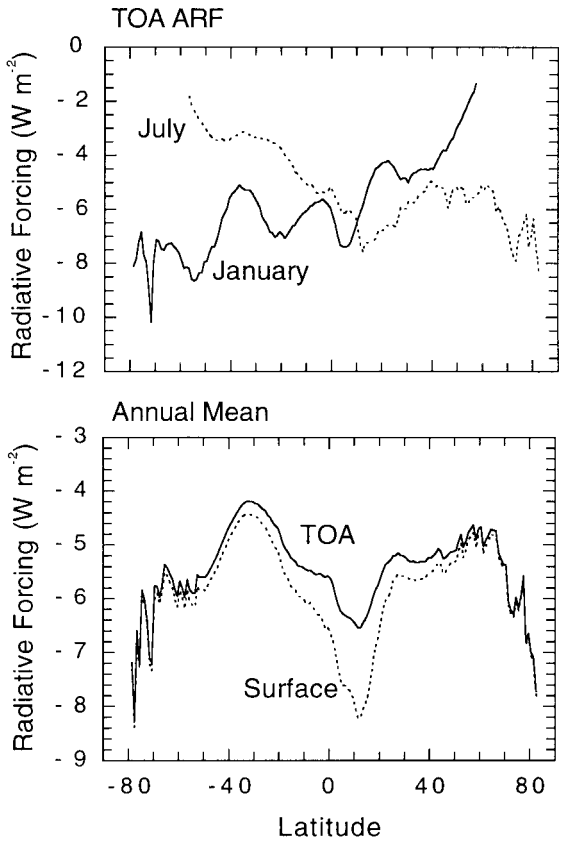

FIG. 5. Latitudinal distributions of the ARF at the TOA in (upper panel) Jan and Jul 1998, and (lower panel) latitudinal distributions of the annual-mean ARF at TOA and the surface for the year 1998.

in the noontime solar zenith angle and the length of day. The upper panel of Fig. 5 shows the TOA ARF in January and July 1998 averaged over oceanic area of respective latitude zones. The cooling at TOA in the summer hemisphere is 6–8 W m^{-2}, but decreases rapidly in the winter hemisphere. Averaged over the year 1998, the two hemispheres are rather symmetric (lower panel). Maximum cooling occurs at high latitudes and in the equatorial region. As can be seen from the difference between the forcing at TOA and the surface, aerosols significantly enhance the solar heating of the atmosphere in the Tropics, with a maximum of ~2 W m^{-2} at 10°N.

During the 1997–98 El Niño period, the big Indonesian fires produced a large amount of aerosols as can be seen from the upper-left panel of Fig. 2. Figure 6 shows that in October 1997 the ARF in the neighborhood of the Maritime Continent reaches −10 W m^{-2} at TOA and −25 W m^{-2} at the surface, with an enhanced atmospheric solar heating of 15 W m^{-2}. This large change in the atmospheric and surface radiation budgets over a large area is expected to have a significant impact on the regional and seasonal climate. Generally, the reduced surface heating due to aerosols will reduce the transfer of water vapor and latent heat to the atmosphere. The atmospheric boundary layer will be more stable and

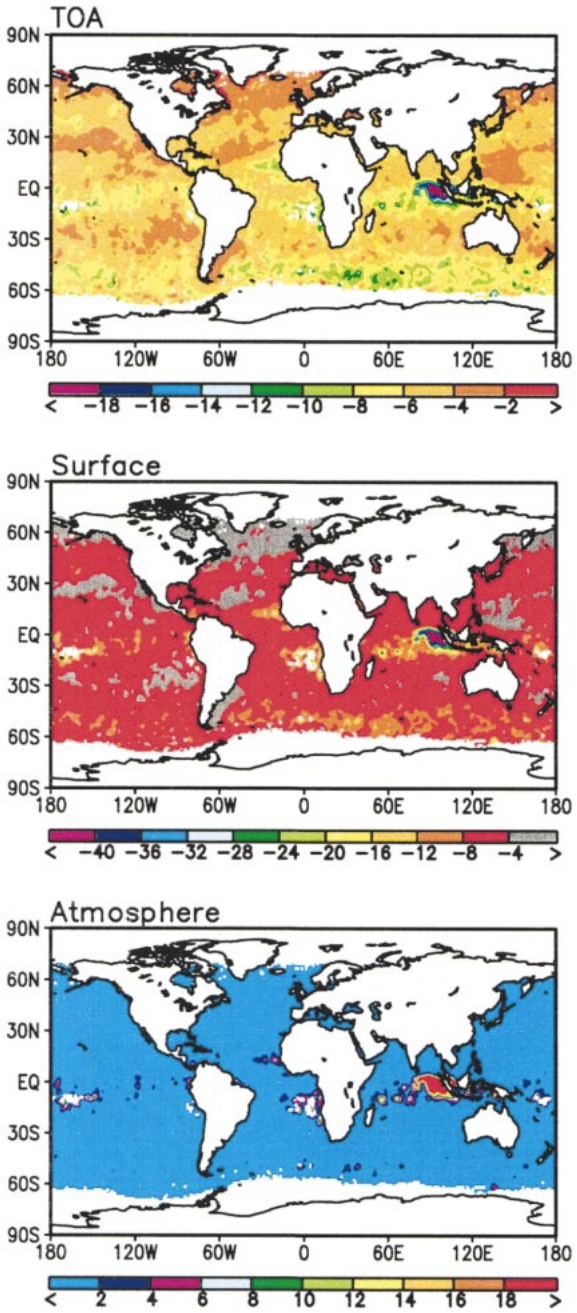

FIG. 6. Aerosol radiative forcing at the TOA, at the surface, and in the atmosphere for the month of Oct 1997, when there were big forest fires in Indonesia. (Units: W m^{-2}.)

the atmospheric circulation is expected to be less rigorous. In a GCM study of the climatic implication of enhanced cloud absorption of solar radiation, Kiehl et al. (1995) found that the extra solar heating of the upper troposphere due to cloud absorption enhanced the stability of the atmosphere, weakened the Hadley circulation, and reduced surface latent heat flux. Since the big 1997–98 Indonesian forest burning lasted for several months and covered a large area, it might have a similar

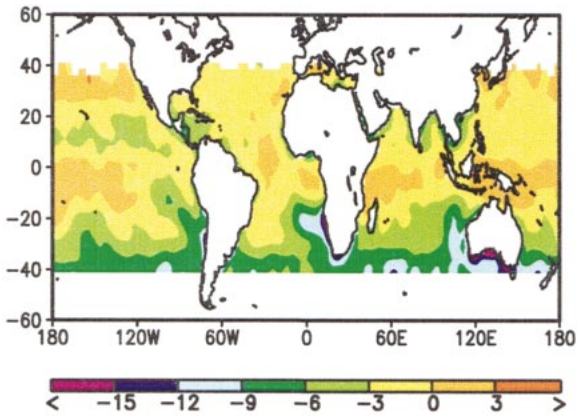

FIG. 7. Difference in clear-sky net downward solar flux at TOA between that retrieved from CERES and that calculated using a radiation model with SeaWiFS-retrieved aerosols (CERES minus model) for Jan 1998. (Units: W m^{-2}.)

effect as the excess cloud absorption of solar radiation in decelerating the hydrological cycle and in strengthening the drought of the region associated with the El Niño.

6. Comparison with CERES clear-sky solar flux

Errors are expected to occur in the model-calculated ARF due to uncertainties in the aerosol optical thickness, single scattering albedo, and asymmetry factor, as well as the radiative transfer parameterization. It is desirable to compare model calculations with satellite-retrieved fluxes at the TOA. The clear-sky TOA fluxes derived from the CERES on the Tropical Rainfall Measuring Mission (TRMM) satellite covers a period of 8 months, from January to August 1998. The data has a temporal resolution of 1 month and a spatial resolution of 2.5° × 2.5° latitude–longitude. The TRMM satellite is a polar-orbiting satellite with a low inclination angle. The CERES only retrieves TOA fluxes at middle and low latitudes between 40°S and 40°N. In Fig. 7, we compare the model-calculated net downward clear-sky solar flux with that of CERES (CERES minus model) for January 1998. Near coastal areas, most of the 2.5° × 2.5° latitude–longitude grids of the CERES span both land and ocean, and $F^{\downarrow}$ is the average value over land and ocean. It cannot be compared directly with the model calculations, which have a spatial resolution of 1° × 1° latitude–longitude and cover only oceanic regions. Therefore, we delete those coastal regions with a difference in $F^{\downarrow}$ greater than 10 W m^{-2}. As can be seen in the figure, the difference is generally within 3 W m^{-2}. Large discrepancy is found in the southern extratropics where the CERES-retrieved $F^{\downarrow}$ is smaller than that of model calculations by more than 6 W m^{-2}. With the coastal regions excluded, the difference in $F^{\downarrow}$ averaged over the ocean from 40°S to 40°N is −1.9 W m^{-2}. Considering the uncertainty in both CERES-de-

rived and model-calculated $F^{\downarrow}$, this difference can be considered small.

7. Conclusions

The direct aerosol radiative forcing over global oceans is calculated using the solar radiation model of Chou and Suarez (1999) and the aerosol optical properties retrieved by the SeaWiFS. Other data input to the radiation model include the column water vapor retrieved from SSM/I radiance measurements, the climatological monthly mean column ozone amount retrieved from TOMS, and the temperature field from the NCEP–NCAR reanalysis.

The aerosol distribution is largely zonal. The large-scale distribution coincides well with the convergence of low-level winds. Large aerosol optical thickness τ_o is found in the equatorial region, Southern Hemispheric high latitudes, Arabian Sea, Bay of Bengal, and the coastal region of the Southeast and East Asia. Minimum τ_o is found in the subtropical divergence zones, especially in the SH. The large τ_o found in the tropical Atlantic persists through most of the year. The prevailing trade winds carry the desert dusts across the Atlantic from Africa to the coasts of Central and South America. The influence of winds on the aerosol distribution is in resemblance of humidity distribution. Aerosol optical thickness is high in convergence zones and low in divergence zones. Averaged over a year, the mean and median of the SeaWiFS-retrieved τ_o at 0.865 μm are both 0.105.

Over global oceans, the annual mean ARF is -5.4 W m^{-2} at TOA and -5.9 W m^{-2} at the surface. The seasonal variation of the ARF is small for global oceans, but it is large for individual hemispheres. The TOA ARF increases by 33% from October to April in the NH and by 50% from July to January in the SH. The clear-sky TOA ARF of -5.4 W m^{-2} is equivalent to a cooling of $\sim$2.5 W m^{-2} when the fractional area of clear-sky regions is taken into consideration. This magnitude of the aerosol cooling is comparable to the warming due to a doubling of the atmospheric CO_2, which is $\sim$4 W m^{-2}.

The ARF during the 1997 Indonesian big forest fires is very large. Over a large area in the vicinity of the Maritime Continent, the cooling due to aerosols in the period September–November 1997 is more than 10 W m^{-2} at TOA and more than 25 W m^{-2} at the surface. Aerosols enhance the solar heating of the atmosphere by $\sim$15 W m^{-2}. The 1997 Indonesian big forest fires occurred during the 1997–98 El Niño event, when the Maritime Continent was under the influence of subsiding air mass and was in drought conditions. The enhanced atmospheric heating and the surface cooling caused by the aerosols of biomass burning could have the effects of increasing atmospheric stability, weakening the atmospheric circulation, and augmenting the drought condition. It would be interesting to study the interactions between the ARF of the biomass burning and the dynamics during an El Niño event using climate model simulations.

Acknowledgments. This work was supported by the Radiation Sciences Program (MDC and PKC) and the SIMBIOS Project (MHW), NASA Office of Earth Science. The aerosol data were produced and distributed, respectively, by the SeaWiFS Project and the Distributed Active Archive Center at the NASA Goddard Space Flight Center. The winds and temperature fields were taken from the NCEP–NCAR reanalysis archive. The SSM/I-retrieved total precipitable water was produced by Remote Sensing Systems sponsored, in part, by NASA and NOAA (Principal Investigator: Frank Wentz). The CERES data were obtained from the NASA Langley Research Center EOSDIS Distributed Active Archive Center.

REFERENCES

Boucher, O., and D. Tanre, 2000: Estimation of the aerosol perturbation to the Earth's radiative budget over oceans using POLDER satellite aerosol retrievals. *Geophys. Res. Lett.*, **27,** 1103–1106.

Chiapello, I., P. Goloub, D. Tanre, and A. Marchand, 2000: Aerosol detection by TOMS and POLDER over oceanic regions. *J. Geophys. Res.*, **105,** 7133–7142.

Chin, M., and Coauthors, 2002: Tropospheric aerosol optical thickness from the GOCART model and comparisons with satellite and sun photometer measurements. *J. Atmos. Sci.*, **59,** 461–483.

Chou, M.-D., and M. J. Suarez, 1999: A solar radiation parameterization for atmospheric studies. NASA Tech. Memo. 1999-104606, 40 pp.

Deuze, J. L., M. Herman, P. Goloub, D. Tanre, and A. Marchand, 1999: Characterization of Aerosols over ocean from POLDER/ADEOS-1. *Geophys. Res. Lett.*, **26,** 1421–1424.

Gordon, H. R., and M. Wang, 1992: Surface roughness considerations for atmospheric correction of ocean color sensors. 1: The Rayleigh scattering component. *Appl. Opt.*, **31,** 4247–4260.

——, and ——, 1994a: Influence of oceanic whitecaps on atmospheric correction of ocean-color sensor. *Appl. Opt.*, **33,** 7754–7763.

——, and ——, 1994b: Retrieval of water-leaving radiance and aerosol optical thickness over the oceans with SeaWiFS: A preliminary algorithm. *Appl. Opt.*, **33,** 443–452.

Gras, J. L., J. B. Jensen, K. Okada, M. Ikegami, Y. Zaizen, and Y. Makino, 1999: Some optical properties of smoke aerosol in Indonesia and tropical Australia. *Geophys. Res. Lett.*, **26,** 1393–1396.

Haywood, J. M., V. Ramaswamy, and B. J. Soden, 1999: Tropospheric aerosol climate forcing in clear-sky satellite observations over the oceans. *Science*, **283,** 1299–1303.

Herman, J. R., P. K. Bhartia, O. Torres, C. Hsu, C. Seftor, and E. Celarier, 1997: Global distribution of UV-absorbing aerosols from *Nimbus-7*/TOMS data. *J. Geophys. Res.*, **102,** 16 911–16 922.

Holben, B. N., and Coauthors, 1998: AERONET—A federated instrument network and data archive for aerosol characterization. *Remote Sens. Environ.*, **66,** 1–16.

Hooker, S. B., W. E. Esaias, G. C. Feldman, W. W. Gregg, and C. R. McClain, 1992: An overview of SeaWiFS and ocean color. NASA Tech Memo. 104566, NASA Goddard Space Flight Center SeaWiFS Tech. Rep. Series, Vol. 1, 24 pp.

Husar, R. B., J. M. Prospero, and L. L. Stowe, 1997: Characterization of tropospheric aerosols over the oceans with the NOAA Advanced Very High Resolution Radiometer optical thickness operational product. *J. Geophys. Res.*, **102,** 16 889–16 909.

Kalnay, E., and Coauthors, 1996: The NCEP/NCAR 40-Year Reanalysis Project. *Bull. Amer. Meteor. Soc.*, **77,** 437–471.

Kaufman, Y. J., B. N. Holben, D. Tanre, I. Slutsker, A. Smirnov, and T. F. Eck, 2000: Will aerosol measurements from *Terra* and *Aqua* polar orbiting satellites represent the daily aerosol abundance and properties? *Geophys. Res. Lett.*, **27,** 3861–3864.

Kiehl, J. T., J. J. Hack, M. H. Zhang, and R. D. Cess, 1995: Sensitivity of a GCM climate to enhanced shortwave cloud absorption. *J. Climate*, **8,** 2200–2212.

McPeters, R. D., and Coauthors, 1998: Earth Probe Total Ozone Mapping Spectrometer (TOMS) data products user's guide. NASA Ref. Publ. 1998-206895, 64 pp.

Mishchenko, M. I., I. V. Geogdzhayev, B. Cairns, W. B. Rossow, and A. A. Lacis, 1999: Aerosol retrievals over the ocean by use of channels 1 and 2 AVHRR data: Sensitivity analysis and preliminary results. *Appl. Opt.*, **38,** 7325–7341.

Podgorny, I. A., W. Conant, V. Ramanathan, and K. Satheesh, 2000: Aerosol modulation of atmospheric and surface solar heating over the tropical Indian Ocean. *Tellus*, **52B,** 947–958.

Rajeev, K., V. Ramanathan, and J. Meywerk, 2000: Regional aerosol distribution and its long-range transport over the Indian Ocean. *J. Geophys. Res.*, **105,** 2029–2043.

Shettle, E. P., and R. W. Fenn, 1979: Models for the aerosols of the lower atmosphere and the effects of humidity variations on their optical properties. U.S. Air Force Geophysics Laboratory Tech. Rep. AFGL-TR-79-0214, 94 pp.

Siegel, D. A., M. Wang, S. Maritorena, and W. Robinson, 2000: Atmospheric correction of satellite ocean color imagery: The black pixel assumption. *Appl. Opt.*, **39,** 3582–3591.

Tegen, I., A. A. Lacis, and I. Fung, 1996: The influence on climate forcing of mineral aerosols from disturbed soils. *Nature*, **380,** 419–422.

——, D. Koch, A. A. Lacis, and M. Sato, 2000: Trends in tropospheric aerosol loads and corresponding impact on direct radiative forcing between 1950 and 1990: A model study. *J. Geophys. Res.*, **105,** 26 971–26 989.

Wang, M., S. Bailey, and C. R. McClain, 2000a: SeaWiFS provides unique global aerosol optical property data. *Eos, Trans. Amer. Geophys. Union*, **81,** 197–202.

——, ——, C. Pietras, C. R. McClain, and T. Riley, 2000b: SeaWiFS aerosol optical thickness matchup analyses. NASA Tech. Memo. 2000-206892, NASA Goddard Space Flight Center SeaWiFS Postlaunch Tech. Rep. Series, Vol. 10, 39–44.

Wentz, F. J., 1994: User's manual SSM/I-2 geophysical tapes. Remote Sensing Systems Tech. Rep. 070194, 20 pp.

Wielicki, B. A., B. R. Barkstrom, E. F. Harrison, R. B. Lee III, G. L. Smith, and J. E. Cooper, 1996: Clouds and the Earth's Radiant Energy System (CERES): An earth observing system experiment. *Bull. Amer. Meteor. Soc.*, **77,** 853–868.

Yang, H., and H. R. Gordon, 1997: Remote sensing of ocean color: Assessment of water-leaving radiance bi-directional effects on atmospheric diffuse transmittance. *Appl. Opt.*, **36,** 7887–7897.